BIOCHEMISTRY
including biophysical chemistry & molecular biology

Article

pubs.acs.org/biochemistry

Structural, Kinetic and Chemical Mechanism of Isocitrate Dehydrogenase-1 from *Mycobacterium tuberculosis*

Christine E. Quartararo, Saugata Hazra, Timin Hadi, and John S. Blanchard*

Department of Biochemistry, Albert Einstein College of Medicine, 1300 Morris Park Avenue, Bronx, New York 10461, United States

Supporting Information

ABSTRACT: *Mycobacterium tuberculosis* (Mtb) is the leading cause of death due to a bacterial infection. The success of the Mtb pathogen has largely been attributed to the nonreplicating, persistence phase of the life cycle, for which the glyoxylate shunt is required. In *Escherichia coli*, flux through the shunt is controlled by regulation of isocitrate dehydrogenase (ICDH). In Mtb, the mechanism of regulation is unknown, and currently, there is no mechanistic or structural information about ICDH. We optimized expression and purification to a yield sufficiently high to perform the first detailed kinetic and structural studies of Mtb ICDH-1. A large solvent kinetic isotope effect [$^{D_2O}V = 3.0 \pm 0.2$, and $^{D_2O}(V/K_{isocitrate}) = 1.5 \pm 0.3$] and a smaller primary kinetic isotope effect [$^{D}V = 1.3 \pm 0.1$, and $^{D}(V/K_{[2R\text{-}^2H]isocitrate}) = 1.5 \pm 0.2$] allowed us to perform the first multiple kinetic isotope effect studies on any ICDH and suggest a chemical mechanism. In this mechanism, protonation of the enolate to form product α-ketoglutarate is the rate-limiting step. We report the first structure of Mtb ICDH-1 to 2.18 Å by X-ray crystallography with NADPH and Mn^{2+} bound. It is a homodimer in which each subunit has a Rossmann fold, and a common top domain of interlocking β sheets. Mtb ICDH-1 is most structurally similar to the R132H mutant human ICDH found in glioblastomas. Similar to human R132H ICDH, Mtb ICDH-1 also catalyzes the formation of α-hydroxyglutarate. Our data suggest that regulation of Mtb ICDH-1 is novel.

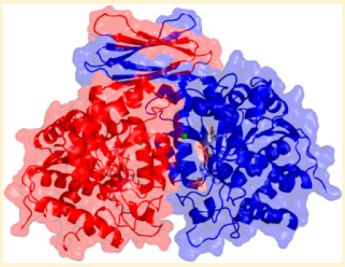

Isocitrate dehydrogenase (ICDH), an enzyme in the tricarboxylic acid (TCA) cycle, catalyzes the oxidative decarboxylation of isocitrate using $NAD(P)^+$ as a cosubstrate to form α-ketoglutarate (αKG), CO_2, and NADPH. In organisms possessing the glyoxylate shunt, which is not present in humans,[1] ICDH sits at a branch point of the TCA cycle and the glyoxylate shunt. Utilization of this shunt is necessary for the virulence and persistence of several organisms,[2] notably in the difficult to treat, nonreplicating physiological phase of *Mycobacterium tuberculosis* (Mtb).[3] This shunt bypasses the two decarboxylative steps of the TCA cycle, allowing organisms to survive under nutrient-limiting conditions, for example, in the persistence phase of the Mtb life cycle.[3] Understanding ICDH, which presumably regulates flux into the glyoxylate shunt, will allow for the development of inhibitors against the shunt, and thus against persistent Mtb. Exploration of new drug targets in persistence is especially important because this phase of the life cycle is nonreplicating, and replication is currently the target of the majority of antibiotics.[4] In *Escherichia coli*, the fate of the isocitrate molecule, either through the glyoxylate shunt or through the TCA cycle, is regulated by the phosphorylation of ICDH by the kinase phosphatase AceK.[5−7] Phosphorylation inactivates ICDH, and isocitrate is funneled instead through isocitrate lyase, the first enzyme of the glyoxylate shunt. No proteins analogous to *E. coli* AceK, or any phosphorylation sites on Mtb ICDH, have been identified. This suggests an unknown mechanism is at play and creates a need and opportunity for research on Mtb ICDH.

The questions surrounding the Mtb TCA cycle do not stop there. Mtb has two ICDHs, the 45.5 kDa ICDH-1 and the 82.6 kDa ICDH-2, both of which are $NADP^+$-dependent.[8] Mtb ICDH-1 and ICDH-2 have differing kinetic parameters under several conditions, including pH, temperature, and salt concentration, suggesting that each isoform may play a role in the diverse environmental conditions confronted by the bacilli.[8] However, no in vivo studies of the necessity of the two ICDHs have been performed, and the functional relevance of the two isoforms is still unknown. Mtb was thought to lack αKG dehydrogenase,[9] but recent studies have demonstrated αKG dehydrogenase activity.[10] Even if an αKG dehydrogenase exists, it is unclear how or if intermediates are funneled through the usually well-defined TCA cycle. Baughn et al.[11] proposed an α-ketoglutarate ferredoxin oxidoreductase that uses ferredoxin instead of $NADP^+$ as the oxidizing agent in the conversion of αKG to succinyl-CoA. There is also the γ-aminobutyric acid (GABA) shunt in which αKG is aminated to glutamate, decarboxylated to GABA, transaminated to succinic semialdehyde, and oxidized to the TCA intermediate succinate.[12,13] However, metabolic labeling experiments by de Carvalho et al.[14] show a nonstoichiometric amount of flux in carbon sources between αKG and succinate, questioning the continuity of the generally defined TCA cycle in Mtb. If Mtb does not use the TCA cycle for metabolism as usual, the discovery of a unique pathway in central carbon metabolism will be fascinating to basic science and provide a myriad of new drug targets.

Received: January 9, 2013
Revised: February 11, 2013
Published: February 14, 2013

dx.doi.org/10.1021/bi400037w | *Biochemistry* 2013, 52, 1765−1775

In this paper, we provide the first mechanistic study and structural data for Mtb ICDH-1. Currently, one-third of the global population is latently infected with Mtb, 10% percent of whom will develop active tuberculosis in their lifetime.[15] Without an improved understanding of the Mtb TCA cycle and the regulation of the glyoxylate shunt, humans will continue to play idle host for Mtb, harboring the disease for the next generation. Deducing the mechanism and crystal structure of Mtb ICDH-1 provides a molecular platform for the development of ICDH-1 as a potential drug target.

MATERIALS AND METHODS

Materials. Isocitrate for isotope effect studies was synthesized as described below, and concentrations were determined enzymatically. For the rest of the experiments, isocitrate was purchased from Sigma-Aldrich as the DL-isocitric acid trisodium salt hydrate and the concentration was determined by weight. Cloning reagents were from New England Biolabs, and primers were from Invitrogen. DNase and complete EDTA-free protease inhibitor cocktail were from Roche. Deuterium oxide (99.9%) and [2,3-$^2H_2$]fumarate were from Cambridge Isotope Laboratories. Crystallography reagents were from Hampton Research. The remainder of the chemicals were purchased from Sigma-Aldrich.

Cloning, Expression, and Purification of ICDH-1. Cloning and expression were modified from a previously reported protocol.[16] The Mtb *icd1* gene (Rv3339c) was amplified via PCR from H37Rv DNA using the forward primer 5′ GGAATTCCATATGTCCAACGCACCCAAGATA 3′ and the reverse primer 5′ CCCAAGCTTCTAATTGGCCAGCTCCTTTTCC 3′. Restriction sites for NdeI and HindIII are underlined, respectively. The PCR fragment was cloned into a pET-28a(+) vector containing an N-terminal His_6 tag. After sequence verification, the recombinant plasmid was transformed into T7 express competent *E. coli* cells. Six liters of LB containing 30 μg/mL kanamycin was inoculated with a 10 mL overnight starter culture and incubated at 37 °C while being shaken at 200 rpm. At an A_{600} of ∼0.35, cells were induced with 0.1 mM IPTG and incubated at 16 °C overnight, while being shaken. Cells were harvested by centrifugation, and the pellets were resuspended in 25 mM triethanolamine (pH 7.5) containing 50 mM NaCl and 20 mM imidazole (buffer A), and one tablet of EDTA-free protease inhibitor cocktail. The resuspended pellets were then emulsified (EmulsiFlex-C3, Avestin) and centrifuged at 17000 rpm for 35 min. Batch purification was performed with a Ni-NTA agarose column. The column was washed with buffer A, and the protein was eluted with a 0 to 300 mM imidazole gradient in buffer A. The His_6 tag was removed by overnight dialysis in 20 mM Tris (pH 8.0) containing 150 mM NaCl, 2.5 mM $CaCl_2$, 1 mM DTT, and 80 units of thrombin. After cleavage, the protein was concentrated and applied to a HiLoad 26/60 Superdex 200 prep grade size exclusion column run in 50 mM HEPES (pH 7.5), 150 mM NaCl, 5 mM $MnCl_2$, and 5% glycerol. The protein was stored in this buffer at −80 °C. The concentration of ICDH-1 was determined using A_{280} and an extinction coefficient of 67965 M^{-1} cm^{-1}.[17]

Measurement of Enzymatic Activity. The enzymatic activity for the primary reaction was determined by monitoring the conversion of $NADP^+$ to NADPH at 340 nm. Experiments were conducted in a Shimadzu UV-2450 spectrophotometer in 100 mM HEPES (pH 7.5) containing 5 mM $MnCl_2$ and varying amounts of isocitrate and $NADP^+$, in a final reaction volume of 1 mL. Assays were performed at room temperature, and 1 nM ICDH-1 was added to initiate the reaction. Rates were calculated using the molar extinction coefficient of NADPH, 6220 M^{-1} cm^{-1},[18] and the total enzyme concentration (E).

For the secondary reaction, preliminary kinetics were obtained by monitoring the decrease in the level of NADPH and αKG at 340 nm. At high concentrations of αKG, the absorbance of αKG at 340 nm overlaps with that of NADPH. Therefore, we calculated a combined ε_{340} of 6260 M^{-1} cm^{-1} for NADPH and αKG, and we limited the "saturating" amount of αKG to keep A_{340} below 2. The αKG Michaelis−Menten experiment was conducted under steady-state conditions in an Applied Photophysics SX-20 stopped-flow instrument in absorbance mode. Final concentrations were 50 mM HEPES (pH 7.5), 150 mM NaCl, 100 μM NADPH, 1−50 mM αKG, and 500 nM ICDH-1. Five replicates for each point were performed. Because of a nonreproducible signal observed during the first 10 s, data were collected from 15 to 30 s postmixing. The NADPH Michaelis−Menten experiment was performed in the Shimadzu UV-2450 spectrophotometer with 100 mM HEPES (pH 7.5), 40 mM αKG, and 1−50 μM NADPH and initiated with 100 nM ICDH-1. Points were repeated in duplicate. Metal was not included in either of these assays because of the observation of a nonlinear rate upon addition of ICDH-1, which we hypothesize to be due to coordination of the metal ions by the large amounts of αKG. In both assays, rates were calculated using an ε_{340} of 6260 M^{-1} cm^{-1} and the total enzyme concentration (E).

Data Fitting. All data fitting was performed with GraphPad Prism version 5.0d. In all graphs, the points are the means of experimental duplicates, and the error bars are the standard deviation of the replicates. The solid lines are the result of fitting to the denoted equation. The error reported with the fitted values is the standard deviation of the fit and is always rounded up.

Initial Velocity of ICDH-1. Initial kinetic parameters were estimated by saturating with one substrate and varying the concentration of the other substrate. The resulting curve was fit to eq 1

$$v = VS/(K_m + S) \quad (1)$$

where V is the maximal velocity and S is the concentration of the varied substrate.

The initial velocity experiment was conducted at fixed concentrations of isocitrate and varying concentrations of $NADP^+$. The resulting pattern was fit globally to eq 2 for a sequential kinetic mechanism

$$v = (VAB)/(K_{ia}K_b + K_aB + K_bA + AB) \quad (2)$$

where V is the maximal velocity, A and B are the substrate concentrations, K_a and K_b are the respective Michaelis constants for each substrate, and K_{ia} is the inhibition constant for substrate A.

Inhibition. Product inhibition by αKG and NADPH and inhibition by malate were tested with variable amounts of inhibitor and varying concentrations of both isocitrate and $NADP^+$. Data were globally fit to eq 3 for competitive inhibition and eq 4 for noncompetitive inhibition

$$v = (VS)/[K_m(1 + I/K_{is}) + S] \quad (3)$$

$$v = (VS)/[K_m(1 + I/K_{is}) + S(1 + I/K_{ii})] \quad (4)$$

dx.doi.org/10.1021/bi400037w | Biochemistry 2013, 52, 1765−1775

where S is the varied substrate concentration, I is the inhibitor concentration, K_{is} is the inhibition constant for the slope, K_{ii} is the inhibition constant for the intercept, and K_m is the Michaelis constant of substrate S.

pH Dependence of ICDH-1 Activity. The pH dependence of the kinetic parameters was determined in 100 mM buffer at the desired pH: MES at pH 5.5−6.5 and HEPES at pH 6.5−8.5. The resulting k_{cat} and k_{cat}/K_m data were fit to eq 5, which describes a single pK_a, the negative log of the acid dissociation constant

$$\log y = \log[-c/(1 + 10^{-x}/10^{-pK_a})] \quad (5)$$

where c is the pH-independent plateau value, y is the rate, and x is the pH.

Primary Kinetic Isotope Effects. Primary kinetic isotope effects (KIEs) were measured using [2*R*-^{2}H]isocitrate. [2*R*-^{2}H]-Isocitrate was synthesized first by chemical synthesis of [2-^{2}H]glyoxylate via [2,3-$^2H_2$]tartaric acid and then by enzymatic synthesis of [2*R*-^{2}H]isocitrate from [2-^{2}H]glyoxylate. See Scheme S1 of the Supporting Information for a pictorial representation.

[2,3-$^2H_2$]Tartaric Acid. *N*-Methylmorpholine *N*-oxide (NMO) (1.00 g, 8.54 mmol) was dissolved in 45 mL of a 1:1 THF/H_2O mixture under an argon atmosphere, and osmium tetroxide (4 wt % in H_2O, 0.60 mL, 0.094 mmol) was added. [2,3-$^2H_2$]Fumaric acid (1.00 g, 8.47 mmol) was added to the solution, and the mixture was stirred at 35 °C overnight, after which TLC analysis (5:4:2:1 *n*-BuOH/MeOH/NH_4OH/H_2O mixture) showed the consumption of fumaric acid. Sodium sulfite (0.20 g, 1.59 mmol) was added to the mixture, and THF and some H_2O were removed in vacuo. The remaining solution was washed twice with EtOAc, and the aqueous layer was subsequently concentrated in vacuo. The crude product was redissolved in H_2O and applied to a 10 mL column of Dowex 1X-2 resin (formate form). The resin was washed with H_2O (3 × 25 mL), then 0.7 N formic acid (3 × 25 mL), and finally 1.4 N formic acid (2 × 25 mL). Fractions containing tartaric acid were pooled, and the solution volume was reduced in vacuo. Distilled water was added, and the mixture was concentrated in vacuo; this procedure was repeated multiple times to remove any residual formic acid and gave [2,3-$^2H_2$]tartaric acid (0.70 g, 4.60 mmol, 54%) as a white solid. As expected, no proton signals were observed in the ^{1}H NMR spectrum (D_2O), and the ^{13}C NMR spectrum signals matched literature values.[19]

[2-^{2}H]Glyoxylic Acid. [2-^{2}H]Glyoxylic acid was synthesized using a modified form of an existing published procedure.[19] [2,3-$^2H_2$]Tartaric acid (0.57 g, 3.75 mmol) was dissolved in 10 mL of H_2O, and the resultant solution was cooled to 0 °C. Periodic acid (1.03 g, 4.50 mmol) was dissolved in 5 mL of H_2O and was added dropwise to the solution. After each 1 mL portion of periodic acid had been added, a single ice chip was dropped into the reaction mixture. After the addition of periodic acid was complete, the cooling bath was removed and the reaction mixture was stirred at room temperature and monitored for the disappearance of starting material by TLC analysis (5:4:2:1 *n*-BuOH/MeOH/NH_4OH/H_2O mixture). After 20 min, the reaction was judged to be complete and the solution was concentrated to approximately 3 mL in vacuo and subsequently loaded onto a 5 mL column of Dowex 1X-2 resin (formate form). The resin was washed with H_2O (60 mL) and then with 0.7 N formic acid (100 mL) to elute the glyoxylic acid. Fractions containing glyoxylic acid were pooled, and the volume was reduced in vacuo before additional distilled H_2O was added to the solution; this procedure was repeated multiple times to remove any residual formic acid and give the fully protonated [2-^{2}H]glyoxylic acid (225 mg, 3.00 mmol, 40%). No proton signals were observed in the ^{1}H NMR spectrum (D_2O), and the ^{13}C NMR spectrum signals matched literature values.[19] The product was dissolved in H_2O, and the solution was carefully titrated to pH 7.0 with dilute NaOH and then frozen and lyophilized to give the sodium salt of [2-^{2}H]-glyoxylic acid as a white powder.

[2*R*-^{2}H]Isocitric Acid. Isocitrate lyase (500 μL, 37.5 μM) was added to a 20 mL solution containing 20 mM Tris (pH 7.5), 50 mM [2-^{2}H]glyoxylate, 200 mM succinate, and 5 mM $MgCl_2$. The mixture was left over the weekend at room temperature. Isocitrate lyase was removed when the solution was passed through an Amicon centrifugal filtration device [10K molecular weight cutoff (MWCO)], and the resulting filtrate was applied to a 85 mL column of Dowex 1X4 (formate form) and eluted with a gradient of 400 mL of 0 to 6 N formic acid. Fractions containing [2*R*-^{2}H]isocitrate, as determined enzymatically using the Mtb ICDH-1 assay, were pooled, and the volume of the solution was reduced in vacuo. Distilled H_2O was added and the solution concentrated in vacuo; this procedure was repeated multiple times to remove residual formic acid, giving [2*R*-^{2}H]isocitrate (103 mg, 0.4 mmol, 80%). The mass spectrum was consistent with an increase in mass of 1 unit from the isotopically unlabeled substrate (m/z 192.1 [M − H]$^-$). All mass spectrometry samples were collected on a 12 T Fourier transform ion cyclotron resonance mass spectrometer (Agilent). Protiated isocitrate was enzymatically synthesized from Sigma-Aldrich glyoxylate and subjected to identical purification procedures.

Isotope effect assays were performed with a saturating concentration of $NADP^+$ and varying concentrations of isocitrate and [2*R*-^{2}H]isocitrate. The results were globally fit to eq 6

$$v = (VS)/[K(1 + F_iE_{V/K}) + S(1 + F_iE_V)] \quad (6)$$

where V is the maximal velocity, S is the concentration of isocitrate or [2*R*-^{2}H]isocitrate, F_i is the fraction of isotope (0 or 1), $E_{V/K}$ is the effect on $k_{cat}/K_m - 1$, and E_V is the effect on $k_{cat} - 1$. The pH dependence of the kinetic isotope effects (KIEs) was measured at pH 5.7 in MES and pH 6.5, 7.5, and 8.5 in HEPES.

Solvent Kinetic Isotope Effects. Solvent KIEs were measured with saturating concentrations of $NADP^+$ and varying concentrations of isocitrate and globally fit to eq 6, where $F_i = 0$ for H_2O and $F_i = 0.95$ for D_2O. A viscosity control of 9% glycerol[20] did not show any effect on either V or $V/K_{isocitrate}$ (data not shown). A proton inventory was performed under saturating conditions of both isocitrate and $NADP^+$ in 10% increments from 0 to 90% D_2O.

Multiple Kinetic Isotope Effects. Multiple KIEs were measured with saturating concentrations of $NADP^+$ and varying concentrations of [2*R*-^{2}H]isocitrate in H_2O and 95% D_2O, and varying concentrations of isocitrate and [2*R*-^{2}H]isocitrate in 95% D_2O. Data were globally fit to eq 6.

Transfer of ^{2}H from [2*R*-^{2}H]Isocitrate to [4*R*-4-^{2}H]NADPH. A 1 mL reaction mixture containing 40 mM HEPES (pH 7.5), 5 mM $MnCl_2$, 5 mM isocitrate or [2*R*-^{2}H]isocitrate, 5 mM $NADP^+$, and a catalytic amount of ICDH-1 was prepared. The enzyme was removed using an Amicon centrifugal filtration device (10K MWCO); 500 μL of

filtrate was loaded onto a MonoQ 4.6/100 PE column, washed with water, eluted in 1 M ammonium bicarbonate (B) (0 to 50% B over 48 min, 50 to 100% B from 48 to 49 min, 100% B from 59 to 64 min, and 100 to 0% B from 64 to 65 min), and then washed with water for 10 min. Fractions with absorbance at both 260 and 340 nm were pooled, lyophilized, and redissolved in D_2O for ^1H NMR spectroscopy.

Crystallization, X-ray Data Collection, and Refinement. Crystals of ICDH-1 in complex with NADPH and Mn^{2+} were grown at room temperature using the vapor diffusion method from hanging drops (1 μL of protein at 10 mg/mL, 5 mM NADPH, and 5 mM $MnCl_2$ mixed with 1 μL of reservoir solution) using a reservoir solution that contained 30% PEG 2K and 0.1 M Tris-HCl (pH 8.0). Crystals were cryoprotected with mineral oil. Diffraction data were collected from a single frozen crystal using a RAXIS-IV^{++} detector mounted on a Rigaku RH-200 rotating anode (copper anode) X-ray generator. Data were processed with HKL3000.[21] The structure was determined by molecular replacement using Phenix[22] and the R132H mutant human ICDH structure with PDB entry 3MAS as a search model. The significantly built model (>90%) was completed by iterative cycles fitting in COOT[23] and refinement in Phenix. There is a dimer per asymmetric unit. Structure figures were synthesized using PyMOL.[24] Atomic coordinates and experimental structure factors have been deposited in the Protein Data Bank (entry 4HCX). Data collection and refinement statistics are listed in Table 1.

RESULTS AND DISCUSSION

Expression and Purification. Expression and purification of Mtb ICDH-1 have been notoriously difficult and provided low yields (personal communication). With optimization, we were able to modify the only other previously successful protocol[16] to obtain enough protein for X-ray crystallography. While our lab was not able to obtain a yield as high as that of Banerjee et al.,[16] the most significant increase came after the substitution of emulsification instead of sonication for cell lysis. Expression yielded both soluble and insoluble proteins of the expected mass, with an increase in the soluble fraction after the postinduction temperature was decreased to 16 °C. Initial purification attempts yielded unstable enzyme, which was remedied by the addition of 5 mM $MnCl_2$ to the gel filtration and storage buffers. Enzymatic activity with several divalent cations was tested. The rate was significantly increased with the addition of 5 mM $MgCl_2$ or $MnCl_2$ compared to 5 mM $CaCl_2$ or $ZnCl_2$. When exogenous $MnCl_2$ was added, the rate was increased 12% compared to that with the addition of exogenous $MgCl_2$ (Table S1 of the Supporting Information). Approximately 0.3 mg of soluble, pure ICDH-1 was obtained per liter of culture. SDS–PAGE was used to determine protein-containing fractions that were >95% pure.

Kinetic Mechanism. The first step in determining a chemical mechanism is to see whether the enzyme proceeds by a sequential mechanism, in which there is a central intermediate(s) containing all substrates, or a ping-pong mechanism, in which one substrate is converted to one product before the next substrate is bound. When the $NADP^+$ concentration was varied at fixed, variable isocitrate concentrations and fit to a sequential mechanism (eq 2), the following parameters were determined: $k_{cat} = 33 \pm 2\ s^{-1}$, $K_{NADP^+} = 15 \pm 3$ μM, $K_{isocitrate} = 50 \pm 7$ μM, and $K_{ia} = 144 \pm 23$ μM. On the basis of the intersecting lines in the double-reciprocal plot, a sequential mechanism is proposed.

Table 1. Summary of Data Collection and Refinement Statistics for the WT ICDH1–NADPH–Mn^{2+} Complex

Data Collection[a]	
X-ray source	rotating anode
wavelength (Å)	1.5418 (Cu anode)
temperature (K)	100
resolution range (Å)	50.0–2.18
no. of reflections	45115 (2069)
completeness (%)	99.0 (92.0)
$I/\sigma(I)$	24.04 (3.75)
redundancy	5.3 (4.3)
space group	$P2_12_12_1$
unit cell	
a (Å)	90.14
b (Å)	92.70
c (Å)	102.90
$\alpha = \beta = \gamma$ (deg)	90.0
no. of molecules per asymmetric unit	2
Refinement	
R_{work} (%)	20.74
R_{free} (%)	26.17
no. of atoms	
protein (chain A)	3130
protein (chain B)	3130
NADPH (chain A)	48
NADPH (chain B)	48
water	310
root-mean-square deviation	
bond lengths (Å)	0.008
bond angles (deg)	1.282
average B factor (Å^2)	
overall (chain A)	32.45
protein main chain (chain A)	32.54
protein side chain (chain A)	32.35
overall (chain B)	35.96
protein main chain (chain B)	36.02
protein side chain (chain B)	35.89
NADPH (chain A)	32.90
NADPH (chain B)	39.42
water (chain A)	34.23
water (chain B)	34.68
PDB entry	4HCX

[a]Values for the highest-resolution shell are given in parentheses.

Inhibition studies were performed to determine the order of substrate binding and product release. All patterns and fitted values are listed in Table 2. Product inhibition with NADPH was competitive against $NADP^+$ and noncompetitive against

Table 2. Product Inhibition Patterns for Mtb ICDH-1

experiment	pattern[a]	fitted parameters
NADPH vs $NADP^+$	C	appK_{is} = 6 ± 2 μM
NADPH vs isocitrate	NC	appK_{is} = 10 ± 2 μM
		appK_{ii} = 49 ± 8 μM
αKG vs $NADP^+$	NC	appK_{is} = 22 ± 6 mM
		appK_{ii} = 11 ± 1 mM
malate vs $NADP^+$	NC	appK_{is} = 80 ± 15 mM
		appK_{ii} = 198 ± 19 mM
malate vs isocitrate	NC	appK_{is} = 98 ± 15 mM
		appK_{ii} = 516 ± 114 mM

[a]Abbreviations: C, competitive; NC, noncompetitive.

dx.doi.org/10.1021/bi400037w | Biochemistry 2013, 52, 1765–1775

isocitrate, suggesting $NADP^+$ binds first and NADPH is released last. αKG was noncompetitive against $NADP^+$. Attempts to assess CO_2 inhibition with $NaHCO_3$ and $KHCO_3$ were unsuccessful because of precipitation at amounts smaller than K_i. Our data support a kinetic mechanism in which $NADP^+$ binds first followed by isocitrate to form a ternary complex before conversion to products. Because isocitrate could bind tightly to the divalent metal, we include the possibility that isocitrate can bind to the free enzyme (Scheme 1). Random sequential substrate binding has been proposed for

Scheme 1. Proposed Kinetic Mechanism of Mtb ICDH-1

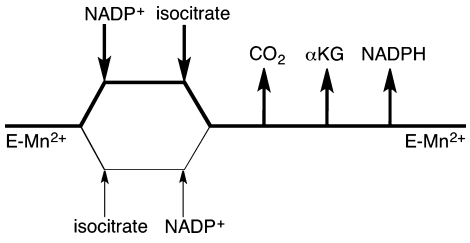

porcine heart mitochondrial ICDH and *E. coli* ICDH.[25−27] Malate was not a substrate and was used as a dead-end inhibitor. It inhibits both $NADP^+$ and isocitrate noncompetitively. It appears that malate can bind to the metal ion in both the E−$NADP^+$ and E−NADPH complexes, yielding effects on both the slope and intercept of the reciprocal plots. Thus, malate inhibition was unable to distinguish between random or ordered substrate binding.

The noncompetitive pattern observed for αKG and $NADP^+$ has two possible interpretations: random product release of CO_2 and αKG or the fact that the ability of αKG to bind free enzyme with or without a nucleotide introduces a slope effect to what would otherwise be uncompetitive inhibition. We prefer the latter interpretation, which we are able to support by additional lines of reasoning. Our inability to demonstrate product inhibition by CO_2, previous reports on the *E. coli* enzyme,[27] and the demonstration of a large solvent KIE due to slow protonation of the metal-liganded αKG enolate anion all support CO_2 as the first product released. Ordered release of αKG and NADPH completes the catalytic cycle.

pH Dependence of ICDH-1. The pH dependence of k_{cat} and k_{cat}/K_m for substrates was tested to explore the ionization states of groups involved in binding and catalysis. Testing was limited at both the upper and lower pH ranges. Above pH 8.5, a reddish-brown precipitate formed. Below pH 5.5, enzyme stability and activity were significantly decreased. When the $NADP^+$ concentration was varied and fit to eq 5, the pK_a of the ionizable group observed for log k_{cat} was 5.6 ± 0.1 and the pK_a of the ionizable group observed for log k_{cat}/K_{NADP^+} was 6.3 ± 0.2 (Figure 1A). When the isocitrate concentration was varied and fit to eq 5, the pK_a of the ionizable group observed for log k_{cat} was 5.5 ± 0.2 (Figure 1B). When analyzing log $k_{cat}/K_{isocitrate}$, we fit the inverse of eq 5 and excluded data at pH 5.5 from the fitting. The pK_a of the ionizable group observed for log $k_{cat}/K_{isocitrate}$ was 5.8 ± 0.1 (Figure 1B). The log k_{cat} values report on the ionization behavior of groups involved in catalysis, while the log k_{cat}/K_m values report on the ionization behavior of groups involved in catalysis and binding. We suggest that the k_{cat}/K_{NADP^+} pH profile is reporting on the binding of $NADP^+$, whose 2′-phosphate is known to have a pK_a of 6.1.[18] When the isocitrate concentration is varied, we suggest that the modest

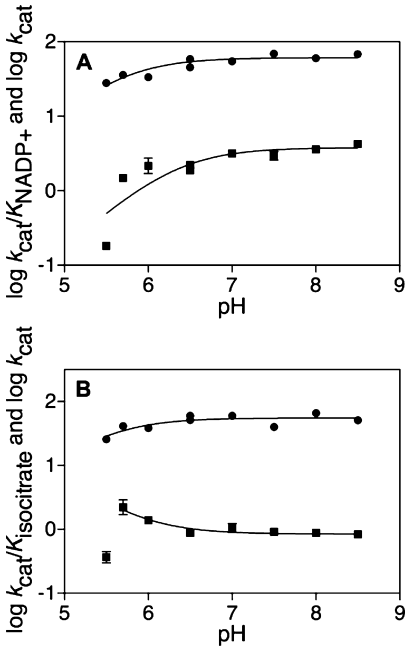

Figure 1. pH dependence of Mtb ICDH-1. (A) k_{cat} and k_{cat}/K_{NADP^+} determined at saturating isocitrate and varying $NADP^+$ concentrations. (●) Fitting log k_{cat} to eq 5 determined pK_a = 5.6 ± 0.1. (■) Fitting log k_{cat}/K_{NADP^+} to eq 5 determined pK_a = 6.3 ± 0.2. (B) k_{cat} and $k_{cat}/K_{isocitrate}$ determined at saturating $NADP^+$ and varying isocitrate concentrations. (●) Fitting log k_{cat} to eq 5 determined pK_a = 5.5 ± 0.2. (■) Fitting log $k_{cat}/K_{isocitrate}$ to the inverse of eq 5 determined pK_a = 5.8 ± 0.1.

increase in $V/K_{isocitrate}$ at pH 5.7 represents the preference of the enzyme for the dianion over the trianion of isocitrate. At the lowest pH values where reliable data could be obtained, k_{cat} decreases modestly, suggesting possible general base catalysis of secondary alcohol oxidation. ICDHs are known to utilize tyrosine as a catalytic acid and lysine as a catalytic base.[28] Aktas and Cook have suggested on the basis of the porcine heart mitochondrial ICDH studies that there is a catalytic triad in which Asp deprotonates Lys to deprotonate the isocitrate C2 hydroxyl, which is not rate-limiting.[28] The Asp may be the source of the hint at the pK_a in the log k_{cat} of 5.5 ± 0.2. Both Lys215 and Tyr142 (Mtb numbering) components of the catalytic triad are conserved (Figure S4 of the Supporting Information). For porcine ICDH-1, it has been suggested that Tyr protonates the intermediate enolate to form product αKG.[29] This is plausible for Mtb ICDH-1 as well (Scheme 2C).

Primary Kinetic Isotope Effects. The primary KIEs with [2*R*-^{2}H]isocitrate were as follows: ^DV = 1.3 ± 0.1 and $^D(V/K_{[2R\text{-}^2H]isocitrate})$ = 1.5 ± 0.2 (Figure 2A). This indicates the transfer of the 2*R* hydrogen of isocitrate to $NADP^+$ is involved in a partially rate-limiting step. In porcine heart ICDH, even smaller kinetic isotope effects with DL-isocitrate-2-(*h*,*d*) were observed, where ^DV and $^D(V/K_{DL\text{-isocitrate-2-}(h,d)})$ were equivalent.[30] However, a nonunity effect occurred at low (4.5) and high (9.5) pH values, with no effect observed at pH 7.45.[30] Because of the pH limitations of the current Mtb assay, the pH dependence of the isotope effects was only tested from pH 5.7 to 8.5 and showed no significant pH dependence of the effect on V or $V/K_{[2R\text{-}^2H]isocitrate}$ (Figure 2B).

Solvent Kinetic Isotope Effects. Solvent KIEs were significantly larger, with a ^{D_2O}V of 3.0 ± 0.2 and a $^{D_2O}(V/K_{isocitrate})$ of 1.5 ± 0.3, indicating that a water-derived proton

dx.doi.org/10.1021/bi400037w | *Biochemistry* 2013, 52, 1765−1775

Scheme 2. Proposed Chemical Mechanism of Mtb ICDH-1

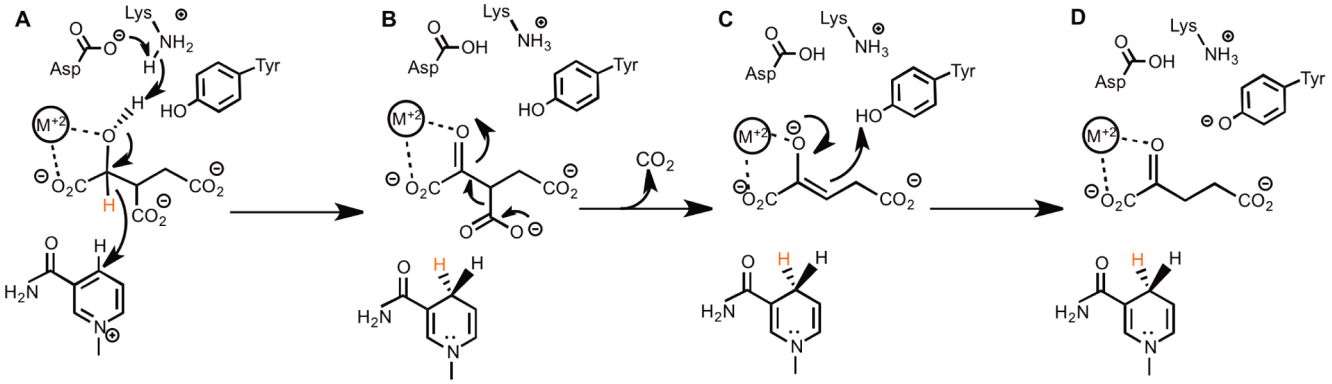

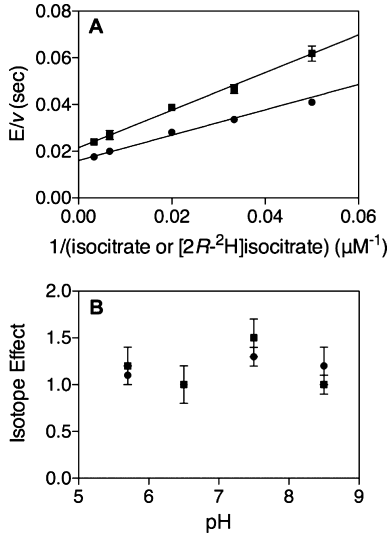

Figure 2. Primary kinetic isotope effects. (A) Primary KIE at 500 μM $NADP^+$ and a varying (20−300 μM) (●) isocitrate or (■) [2*R*-^{2}H]isocitrate concentration. ^{D}V = 1.3 ± 0.1, and $^{D}(V/K_{[2R\text{-}^2H]isocitrate})$ = 1.5 ± 0.2. (B) pH dependence of (●) ^{D}V and (■) $^{D}(V/K_{[2R\text{-}^2H]isocitrate})$ at 500 μM $NADP^+$ and a varying (5−150 μM) isocitrate or [2*R*-^{2}H]isocitrate concentration.

transfer is responsible for a rate-limiting step in catalysis (Figure 3A). A linear proton inventory (Figure 3B) shows that only a single solvent proton is giving rise to this effect. Additionally, when solving for 0% D_2O in the line that was fit to the data ($y = -52.52x + 73.43$) and dividing by the value at 95% D_2O, we obtain a ^{D_2O}V of 3.1, within the error of the experimentally determined ^{D_2O}V.

There are two proton transfer reactions catalyzed by ICDH, the deprotonation of the secondary alcohol, concurrent with or prior to hydride transfer (Scheme 2A), and the protonation of the enolate of αKG after decarboxylation of the oxalosuccinate intermediate (Scheme 2C). For porcine heart ICDH, the authors proposed that the initial deprotonation of the secondary alcohol was the rate-limiting step and source of the large solvent KIE.[31] However, for there to be such a small primary KIE [^{D}V = 1.3 ± 0.1, and $^{D}(V/K_{[2R\text{-}^2H]isocitrate})$ = 1.5 ± 0.2] in Mtb ICDH-1, then the formation and collapse of the alkoxide must be completely uncoupled. Metal coordination of the formed alkoxide would be a stabilizing factor but should also make its formation facile. This same argument applies to the stabilization of the enolate formed after decarboxylation of oxalosuccinate. However, if a strong metal interaction was present, the enolate would be protonated slowly, and this could be the source of the large solvent KIE that we observe. To distinguish between these two possibilities, we performed multiple KIE studies to determine if the deprotonation of the secondary alcohol and the protonation of the enolate occurred in two discrete steps or as a coupled, concerted step. Colman and Chu[31] did not have this luxury because their studies in 1969 predated the advent of multiple KIEs for deducing reaction mechanisms in 1982.[32]

Multiple Kinetic Isotope Effects. Multiple KIEs were measured with isocitrate and [2*R*-^{2}H]isocitrate in 95% D_2O (Figure 3C). Values for ^{D}V of 1.2 ± 0.1 and $^{D}(V/K_{[2R\text{-}^2H]isocitrate})$ of 1.0 ± 0.2 were determined. Because these multiple KIEs are smaller than their value in H_2O [^{D}V = 1.3 ± 0.1, and $^{D}(V/K_{[2R\text{-}^2H]isocitrate})$ = 1.5 ± 0.2], a stepwise mechanism is predicted[32] in which the primary KIE from [2*R*-^{2}H]isocitrate and solvent KIE from D_2O report on two separate steps. Multiple KIEs were also measured with [2*R*-^{2}H]isocitrate in H_2O and 95% D_2O (Figure 3D). Values ^{D_2O}V (1.7 ± 0.2) and $^{D_2O}(V/K_{[2R\text{-}^2H]isocitrate})$ (1.0 ± 0.2) were determined. These values are decreased compared to those with isocitrate [^{D_2O}V = 3.0 ± 0.2, and $^{D_2O}(V/K_{isocitrate})$ = 1.5 ± 0.3], again indicating a stepwise mechanism. The clear data for a stepwise mechanism indicate either that the formation and collapse (Scheme 2A) of the isocitrate alkoxide are completely uncoupled or that the origin of the Mtb ICDH-1 solvent KIE is the protonation of the αKG enolate formed after decarboxylation (Scheme 2C). On the basis of the likely strong stabilization of both anionic intermediates caused by metal ion ligation, we believe that the results of our multiple KIEs are more compatible with protonation of the αKG enolate being the source of the large solvent KIE.

Transfer of ^{2}H from [2*R*-^{2}H]Isocitrate to [4*R*-4-^{2}H]NADPH. The transfer of the deuterium from [2*R*-^{2}H]-isocitrate to the A-side of the nicotinamide ring to form [4*R*-4-^{2}H]NADPH was assessed by ^{1}H NMR spectroscopy (Figure S1A of the Supporting Information). This was the expected result, as other isocitrate dehydrogenases also catalyze an A-side specific transfer.[33] A control reaction was performed with [2*R*-^{1}H]isocitrate (Figure S2B of the Supporting Information). The assignment of stereochemistry of the transfer of deuterium to NADPH was based on previous work by Ottolina et al.[34]

Three-Dimensional Structure of Mtb ICDH-1. We crystallized Mtb ICDH-1 and determined the first three-dimensional structure of Mtb ICDH-1 by molecular replacement using human cytosolic (Hc) ICDH (PDB entry 3MAS) as a template. It is interesting that Mtb ICDH-1 more closely

dx.doi.org/10.1021/bi400037w | *Biochemistry* 2013, 52, 1765−1775

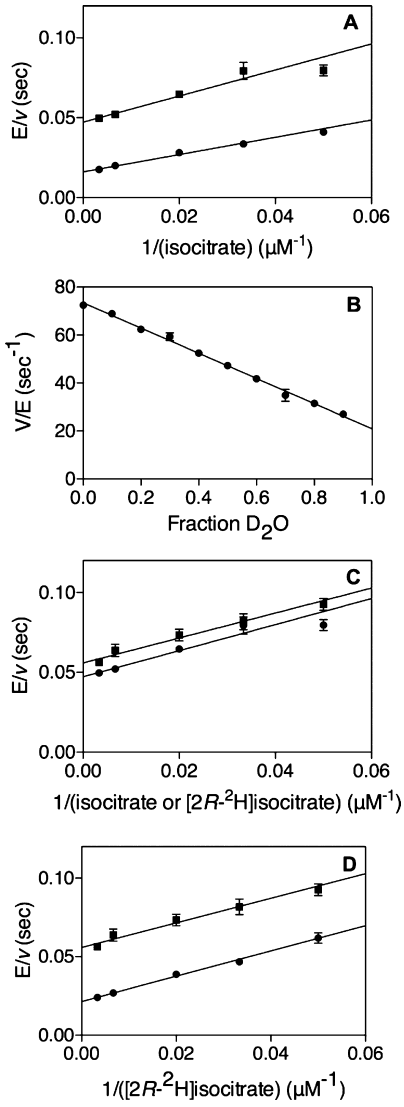

Figure 3. Solvent and multiple kinetic isotope effects. (A) Solvent KIE with 500 μM $NADP^+$ and a varying (20−300 μM) isocitrate concentration in (●) H_2O or (■) 95% D_2O. ^{D_2O}V = 3.0 ± 0.2, and $^{D_2O}(V/K_{isocitrate})$ = 1.5 ± 0.3. (B) Proton inventory in which k_{cat} was measured with 500 μM isocitrate and 500 μM $NADP^+$ at 10% increments of D_2O and fit to a straight line. (C) Multiple KIEs with 500 μM $NADP^+$ and a varying (20−300 μM) (●) isocitrate or (■) [2*R*-^{2}H]isocitrate concentration in 95% D_2O. ^{D}V = 1.2 ± 0.1, and $^{D}(V/K_{[2R\text{-}^2H]isocitrate})$ = 1.0 ± 0.2. (D) Multiple KIEs with 500 μM $NADP^+$ and a varying (20−300 μM) [2*R*-^{2}H]isocitrate concentration in (●) H_2O or (■) 95% D_2O. ^{D_2O}V = 1.7 ± 0.2, and $^{D_2O}(V/K_{[2R\text{-}^2H]isocitrate})$ = 1.0 ± 0.2.

resembles mammalian instead of bacterial ICDHs and further suggests that Mtb ICDH-1 regulation may be drastically different from that in *E. coli*. After several rounds of minimization, the structure was optimized with an R_{work} of 20.7 and an R_{free} of 26.2. The final structure is shown in Figure 4. The Ramachandran plot shows 89.4% of the residues in the most favored region and 9.1% of the residues in allowed regions. Each monomer of Mtb ICDH-1 consists of a bottom globular domain composed primarily of a Rossmann fold, a common dinucleotide binding domain. Above the Rossmann motif, each monomer has two β hairpins connected by a longer loop. Each of these hairpins interacts with the hairpin of the other monomer to form two antiparallel β sheets (Figure 4).

Mtb ICDH-1 exhibits planar symmetry with Mn^{2+} bound toward the center of the plane, represented as a green sphere in Figure 4. As shown for the B chain (Figure 5C), Mn^{2+} is hexagonally coordinated by Asp282 and Asp278 of chain B, Asp255 of chain A, and two water molecules. We propose the coordination of the metal by both monomers enhances dimer formation and stability. In a sequence alignment (Figure S4 of the Supporting Information) of the top three blast hits in the PDB, two of which are mammalian, along with Mtb ICDH-1 and *E. coli* ICDH, Asp282 and Asp278 are conserved in all aligned sequences and Asp255 is conserved in all except *E. coli*.

The NADPH molecules are exclusively bound by residues of the monomer to which they bind. All of the NADPH−Mtb ICDH-1 contacts are conserved in the top three blast hits (Figure S4 of the Supporting Information). NADPH is primarily held in place by various electrostatic and hydrogen bonding interactions. A schematic showing all of the interactions of NADPH and Mtb ICDH-1 is shown in Figure S5 of the Supporting Information. It is worth noting the side chain nitrogens from Arg317 and His318 coordinate the 2′-phosphate on the adenosine ribose. The importance of this interaction is highlighted by the inability of Mtb ICDH-1 to catalyze a detectable reaction using NAD^+ as its cofactor, as shown by Banerjee et al.[8] and repeated in our own lab (data not shown). These interactions are generally on the order of 3 Å, and we predict a collapse of the enzyme active site upon the binding of isocitrate in the cleft (Figure 5B) to strengthen these interactions. The hypothesized structural rearrangement necessary for catalysis entertains the possibility of a structure-based regulatory mechanism of Mtb ICDH-1.

Structural and Regulatory Comparison of Mtb and *E. coli* ICDH. The structural similarity of Mtb ICDH-1 to Hc ICDH suggests that the *E. coli* method of regulation of the glyoxylate shunt may not be applicable to Mtb. *E. coli* ICDH is regulated by phosphorylation of Ser113,[35] which hydrogen bonds to isocitrate in the active site.[36] In Mtb ICDH-1, Glu88 corresponds to the phosphorylated Ser113 in *E. coli* and is located on the outer edge of the protein distant from the active site in the Mtb structure. Recently, the first structure of the "fully closed" *E. coli* ICDH has been determined, indicating *E. coli* ICDH undergoes conformational changes upon substrate binding and providing a structural basis for the previously postulated mechanism.[37]

Structural and Regulatory Comparison of Mtb and Human ICDH. Similar to that of *E. coli*, Hc ICDH is proposed to exist in three conformational states: open, semiopen, and closed.[38] However, Hc ICDH is self-regulated by the transition between these states and not by phosphorylation. It is also important to remember Hc ICDH regulation occurs for a different reason, as the glyoxylate shunt is not present in humans. Initial work to search for the analogous phosphorylation site of *E. coli* ICDH in Hc ICDH proposed Ser94 to be the regulation site corresponding to *E. coli* Ser113. In Hc ICDH, Asp278 interacts with Ser94 to inhibit the activity in the $NADP^+$-bound, open form. In the active, closed form, this interaction is disrupted by a conformational change, from a loop to a helix, of the segment bearing Asp278, which then coordinates Ca^{2+} in the isocitrate−$NADP^+$−Ca^{2+} form to allow enzymatic activity.[38] In the Mtb enzyme, the equivalent of Hc Ser94 is Ser97, and this residue is located on a loop 7.6 Å from the bound NADPH and 12.8 Å directly across the cleft from Asp278, which is coordinating the metal. The location of Mtb Ser97 and Mtb Asp278 across from one another, with no

dx.doi.org/10.1021/bi400037w | *Biochemistry* 2013, 52, 1765−1775

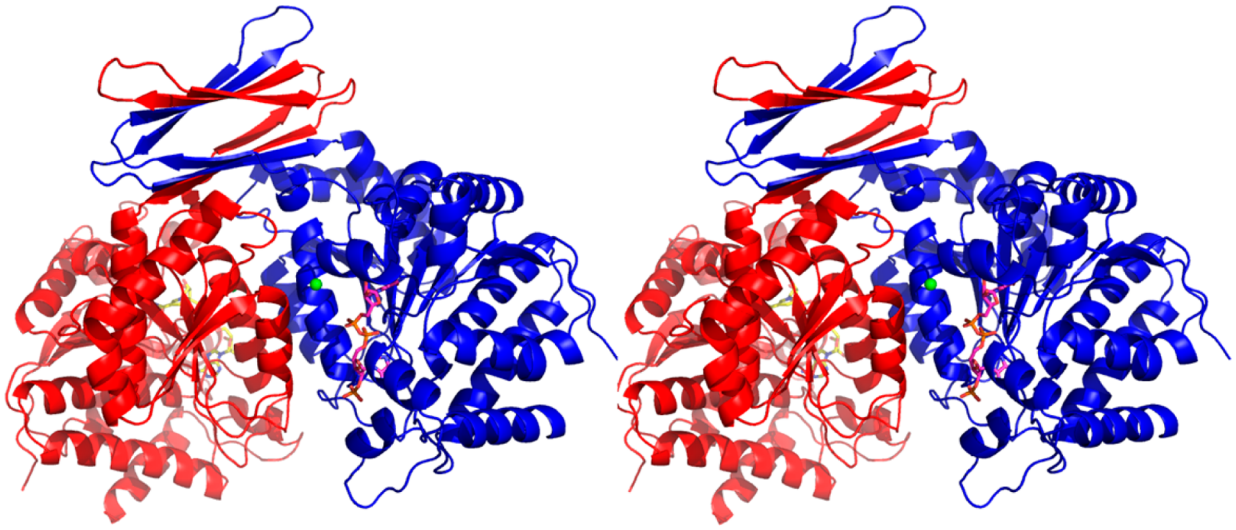

Figure 4. Stereoview of Mtb ICDH-1. Each monomer is bound to one Mn^{2+}, shown as a green sphere, and one NADPH, shown as sticks.

interference from any other residues, suggests that a similar regulatory mechanism, in which Asp278 and Ser97 could interact in a more compact conformation, is at least feasible. However, in our structure, the regulatory segment exists as a helix without isocitrate bound. If this NADPH-bound Mtb ICDH-1 structure represents an open conformation, an analogous Hc ICDH-based regulatory mechanism would have to be tweaked so that this interaction occurred in a semiopen form, as Asp278 and Ser97 are currently too far away to interact in the Mtb structure. Three phosphorylation sites in Mtb ICDH-1 have been proposed using sequence-based computational tools,[39] but to date, there is no experimental evidence of phosphorylation. Neither the *E. coli* nor the Hc ICDH regulatory mechanisms are fully supported by this Mtb structure, suggesting Mtb ICDH-1 may be regulated by a novel mechanism.

The R132H mutation is responsible for the secondary activity of Hc ICDH, converting αKG to α-hydroxyglutarate (αHG) in glioblastomas.[40] R132 is conserved in all aligned ICDHs and is equivalent to Mtb ICDH-1 R135. In our crystal structure, the guanidinium nitrogens of R135 are 5.4 and 6.5 Å from the Mn^{2+}, in the cavity that we propose isocitrate binds. This is not surprising, because human R132 is proposed to be involved in isocitrate binding and the transition to another conformation.[41] Complexes of Mtb ICDH-1 with a catalytic or dead end complex, biochemical studies, and mutagenesis would be necessary to determine the exact role of R135 in Mtb ICDH-1.

Secondary Reaction. In 2009, Dang et al.[40] found that mutant forms of Hc ICDH identified in glioblastomas produced αHG. Subsequent studies by Pietrak et al.[42] found that αHG is also produced, albeit much slower, by the WT Hc ICDH and WT and mutant ICDH from *Azotobacter vinelandii*. This secondary reaction was also observed for WT Mtb ICDH-1 when αKG and NADPH were used as substrates. Subsequently, the formation of αHG was confirmed by mass spectrometry (Figure S2 of the Supporting Information). Preliminary kinetic values were obtained: $k_{cat} \sim 0.1-0.2\ s^{-1}$, $K_{\alpha KG} \sim 8$ mM, and $K_{NADPH} < 4\ \mu M$ (see Figure S3 of the Supporting Information for measurements and associated errors). We are calling these kinetic parameters preliminary because we could not saturate with αKG and no $MnCl_2$ was added. Addition of $MnCl_2$ gave a nonlinear rate, presumably by coordinating αKG. Running the normal reaction without exogenous metal substantially decreased k_{cat} (Table S1 of the Supporting Information). These kinetic parameters support the mass spectrometry evidence of the enzymatic conversion of αKG and NADPH to αHG and $NADP^+$, respectively. A detailed kinetic analysis of this reaction would be an intriguing follow-up. The significance of this reaction for WT Mtb ICDH-1 is unknown at this time.

Proposed Mechanism. As shown in Scheme 2A, isocitrate and $NADP^+$ are both bound to the enzyme before the reaction can commence. On the basis of the pH−rate profile in which log $k_{cat}/K_{isocitrate}$ has an increase at pH 5.7 (Figure 1B), and decreased activity without a divalent metal, isocitrate is proposed to coordinate the Mn^{2+} through its C1 carboxyl and C2 hydroxyl groups. There is a base-assisted deprotonation from the C2 isocitrate hydroxyl, by the lysine group that is deprotonated by an aspartate residue whose pK_a (Figure 1A,B) is observed in the log k_{cat} pH−rate profile. Deprotonation of the C2 isocitrate hydroxyl is coupled to the transfer of a hydride from C2 of isocitrate to the nicotinamide ring to generate the A-side (4*R*) product NADPH that remains bound on the enzyme (Scheme 2A and Figure S1 of the Supporting Information). The intermediate oxalosuccinate (Scheme 2B) undergoes decarboxylation to generate CO_2 and form the metal-stabilized enolate depicted in Scheme 2C. The enolate is then protonated at position C3, by a catalytic acid, likely Tyr, bearing the solvent exchangeable proton giving rise to the large solvent KIE, to yield product αKG (Scheme 2D).

Conclusion. We have provided kinetic and structural evidence of the kinetic and chemical mechanism of Mtb ICDH-1. ICDH-1 catalyzes a sequential reaction in which $NADP^+$ and isocitrate bind to the enzyme to form a ternary complex before conversion to product. Substrate binding is random, but $NADP^+$ preferentially binds first. Product release is ordered with CO_2 released first, followed by αKG, and finally NADPH. The first use of multiple KIE studies for any ICDH determined that protonation of the enolate of αKG, and not the initial deprotonation of the secondary alcohol, as reported for porcine heart ICDH, is the origin of the large solvent KIE. This suggests that catalysis is different in Mtb ICDH-1. The first X-ray crystallographic structure of Mtb ICDH-1 is remarkably

dx.doi.org/10.1021/bi400037w | *Biochemistry* 2013, 52, 1765−1775

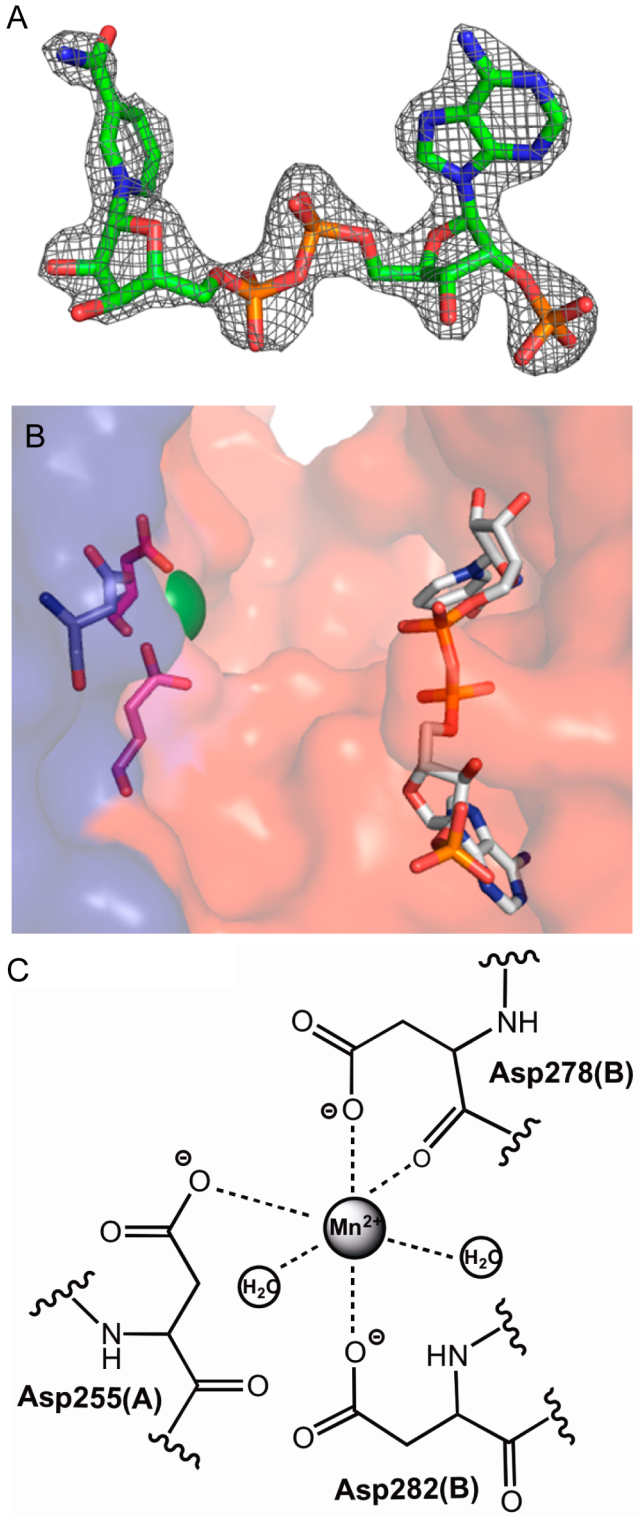

Figure 5. Ligands in the Mtb ICDH-1 structure. (A) Electron density map for NADPH contoured at 2σ. (B) Close-up of one of the two the active sites showing Mn^{2+} as a green sphere and NADPH as sticks. Coordinating residues of the Mn^{2+} from the A chain are colored pink, and the residue from the B chain is colored blue. (C) Metal binding site.

similar to that of Hc ICDH, making it unlikely that regulation of this enzyme proceeds in the same manner as that of *E. coli*. Further similarity to R132H Hc ICDH was observed in the presence of a secondary reaction to form αHG. The expression, purification, and crystallization conditions of Mtb ICDH-1 presented in this work should facilitate determination of the structure of Mtb ICDH-1 in complex with Mn^{2+}-isocitrate, Mn^{2+}-isocitrate-NADPH, or an inhibitory or dead-end complex. All of these complexes are necessary in studying the regulatory mechanism of Mtb ICDH-1 through a structural approach. The biochemical and structural studies in this paper have allowed us to propose a chemical mechanism for Mtb ICDH-1. This is a critical building block for the full comprehension of the persistence phase of Mtb and for inhibitor development against the nonreplicating bacilli.

■ ASSOCIATED CONTENT

Ⓢ Supporting Information

A table of rates using different divalent cations (Table S1), the reaction scheme of [2*R*-^{2}H]isocitrate synthesis (Scheme S1), identification of products of [4*R*-4-^{2}H]NADPH by NMR (Figure S1) and αHG by mass spectrometry (Figure S2), kinetics of the secondary reaction (Figure S3), a sequence alignment of other ICDHs (Figure S4), and NADPH−Mtb ICDH-1 contacts (Figure S5). This material is available free of charge via the Internet at http://pubs.acs.org.

Accession Codes

Coordinates have been deposited as PDB entry 4HCX.

■ AUTHOR INFORMATION

Corresponding Author

*Department of Biochemistry, Albert Einstein College of Medicine, 1300 Morris Park Ave., Bronx, NY 10461. Phone: (718) 430-3096. Fax: (718) 430-8565. E-mail: john.blanchard@einstein.yu.edu.

Funding

This work was supported by National Institutes of Health Grants AI33696 to J.S.B. and T32 AI007501 to C.E.Q.

Notes

The authors declare no competing financial interest.

■ ACKNOWLEDGMENTS

We thank Dr. Hui Xiao for performing the mass spectrometric identification of αHG and Dr. Michael Brenowitz for performing analytical ultracentrifugation studies not included in this paper. We thank members of the laboratory of Dr. Steven Almo, particularly Dr. Matthew Vetting, Rafael Toro, and Rahul Bhosle, for their helpful suggestions and expertise.

■ ABBREVIATIONS

DTT, dithiothreitol; EDTA, ethylenediaminetetraacetic acid; HEPES, *N*-(2-hydroxyethyl)piperazine-*N*′-2-ethanesulfonic acid; IPTG, isopropyl β-D-thiogalactopyranoside; LB, Luria broth; MES, 2-(*N*-morpholino)ethanesulfonic acid; MWCO, molecular weight cutoff; Ni-NTA, nickel nitriloacetic acid; NMR, nuclear magnetic resonance; PCR, polymerase chain reaction; PDB, Protein Data Bank; SDS−PAGE, sodium dodecyl sulfate−polyacrylamide gel electrophoresis; Tris, tris(hydroxymethyl)aminomethane; WT, wild type.

■ REFERENCES

(1) Kondrashov, F. A., Koonin, E. V., Morgunov, I. G., Finogenova, T. V., and Kondrashova, M. N. (2006) Evolution of glyoxylate cycle enzymes in Metazoa: Evidence of multiple horizontal transfer events and pseudogene formation. *Biol. Direct 1*, 31.

(2) Dunn, M. F., Ramirez-Trujillo, J. A., and Hernandez-Lucas, I. (2009) Major roles of isocitrate lyase and malate synthase in bacterial and fungal pathogenesis. *Microbiology 155*, 3166−3175.
(3) McKinney, J. D., Honer zu Bentrup, K., Munoz-Elias, E. J., Miczak, A., Chen, B., Chan, W. T., Swenson, D., Sacchettini, J. C., Jacobs, W. R., Jr., and Russell, D. G. (2000) Persistence of *Mycobacterium tuberculosis* in macrophages and mice requires the glyoxylate shunt enzyme isocitrate lyase. *Nature 406*, 735−738.
(4) Zhang, Y. (2005) The magic bullets and tuberculosis drug targets. *Annu. Rev. Pharmacol. Toxicol. 45*, 529−564.
(5) LaPorte, D. C., and Chung, T. (1985) A single gene codes for the kinase and phosphatase which regulate isocitrate dehydrogenase. *J. Biol. Chem. 260*, 15291−15297.
(6) Garnak, M., and Reeves, H. C. (1979) Phosphorylation of Isocitrate dehydrogenase of *Escherichia coli*. *Science 203*, 1111−1112.
(7) LaPorte, D. C., and Koshland, D. E., Jr. (1982) A protein with kinase and phosphatase activities involved in regulation of tricarboxylic acid cycle. *Nature 300*, 458−460.
(8) Banerjee, S., Nandyala, A., Podili, R., Katoch, V. M., and Hasnain, S. E. (2005) Comparison of *Mycobacterium tuberculosis* isocitrate dehydrogenases (ICD-1 and ICD-2) reveals differences in coenzyme affinity, oligomeric state, pH tolerance and phylogenetic affiliation. *BMC Biochem. 6*, 20.
(9) Tian, J., Bryk, R., Shi, S., Erdjument-Bromage, H., Tempst, P., and Nathan, C. (2005) *Mycobacterium tuberculosis* appears to lack α-ketoglutarate dehydrogenase and encodes pyruvate dehydrogenase in widely separated genes. *Mol. Microbiol. 57*, 859−868.
(10) Wagner, T., Bellinzoni, M., Wehenkel, A., O'Hare, H. M., and Alzari, P. M. (2011) Functional plasticity and allosteric regulation of α-ketoglutarate decarboxylase in central mycobacterial metabolism. *Chem. Biol. 18*, 1011−1020.
(11) Baughn, A. D., Garforth, S. J., Vilcheze, C., and Jacobs, W. R., Jr. (2009) An anaerobic-type α-ketoglutarate ferredoxin oxidoreductase completes the oxidative tricarboxylic acid cycle of *Mycobacterium tuberculosis*. *PLoS Pathog. 5*, e1000662.
(12) Rhee, K. Y., de Carvalho, L. P., Bryk, R., Ehrt, S., Marrero, J., Park, S. W., Schnappinger, D., Venugopal, A., and Nathan, C. (2011) Central carbon metabolism in *Mycobacterium tuberculosis*: An unexpected frontier. *Trends Microbiol. 19*, 307−314.
(13) de Carvalho, L. P., Ling, Y., Shen, C., Warren, J. D., and Rhee, K. Y. (2011) On the chemical mechanism of succinic semialdehyde dehydrogenase (GabD1) from *Mycobacterium tuberculosis*. *Arch. Biochem. Biophys. 509*, 90−99.
(14) de Carvalho, L. P., Fischer, S. M., Marrero, J., Nathan, C., Ehrt, S., and Rhee, K. Y. (2010) Metabolomics of *Mycobacterium tuberculosis* reveals compartmentalized co-catabolism of carbon substrates. *Chem. Biol. 17*, 1122−1131.
(15) World Health Organization (2012) Tuberculosis, Fact Sheet 104. http://www.who.int/mediacentre/factsheets/fs104/en/index.html.
(16) Banerjee, S., Nandyala, A., Podili, R., Katoch, V. M., Murthy, K. J., and Hasnain, S. E. (2004) *Mycobacterium tuberculosis* (Mtb) isocitrate dehydrogenases show strong B cell response and distinguish vaccinated controls from TB patients. *Proc. Natl. Acad. Sci. U.S.A. 101*, 12652−12657.
(17) ExPASy (2011) ProtParam Tool. http://ca.expasy.org/tools/protparam.html (accessed June 15).
(18) *The Merck Index*, 14th ed. (2006) Merck & Co., Inc., Whitehouse Station, NJ.
(19) Lobell, M., and Crout, D. H. G. (1996) New insight into the pyruvate decarboxylase-catalysed formation of lactaldehyde from H-D exchange experiments: a 'water proof' site. *J. Chem. Soc., Perkin Trans. 1*, 1577−1581.
(20) Karsten, W. E., Lai, C. J., and Cook, P. F. (1995) Inverse Solvent Isotope Effects in the NAD-Malic Enzyme Reaction Are the Result of the Viscosity Difference between D_2O and H_2O: Implications for Solvent Isotope Effect Studies. *J. Am. Chem. Soc. 117*, 5914−5918.
(21) Otwinowski, Z., and Minor, W. (1997) Processing of X-ray diffraction data collected in oscillation mode. In *Methods in Enzymology* (Carter, C. W., Jr., Ed.) pp 307−326, Academic Press, San Diego.
(22) Adams, P. D., Gopal, K., Grosse-Kunstleve, R. W., Hung, L. W., Ioerger, T. R., McCoy, A. J., Moriarty, N. W., Pai, R. K., Read, R. J., Romo, T. D., Sacchettini, J. C., Sauter, N. K., Storoni, L. C., and Terwilliger, T. C. (2004) Recent developments in the PHENIX software for automated crystallographic structure determination. *J. Synchrotron Radiat. 11*, 53−55.
(23) Emsley, P., and Cowtan, K. (2004) Coot: Model-building tools for molecular graphics. *Acta Crystallogr. 60*, 2126−2132.
(24) DeLano, W. L. (2002) *The PyMOL Molecular Graphics System*, DeLano Scientific, San Carlos, CA.
(25) Uhr, M. L., Thompson, V. W., and Cleland, W. W. (1974) The kinetics of pig heart triphosphopyridine nucleotide-isocitrate dehydrogenase. I. Initial velocity, substrate and product inhibition, and isotope exchange studies. *J. Biol. Chem. 249*, 2920−2927.
(26) Northrop, D. B., and Cleland, W. W. (1974) The kinetics of pig heart triphosphopyridine nucleotide-isocitrate dehydrogenase. II. Dead-end and multiple inhibition studies. *J. Biol. Chem. 249*, 2928−2931.
(27) Dean, A. M., and Koshland, D. E., Jr. (1993) Kinetic mechanism of *Escherichia coli* isocitrate dehydrogenase. *Biochemistry 32*, 9302−9309.
(28) Aktas, D. F., and Cook, P. F. (2009) A lysine-tyrosine pair carries out acid-base chemistry in the metal ion-dependent pyridine dinucleotide-linked β-hydroxyacid oxidative decarboxylases. *Biochemistry 48*, 3565−3577.
(29) Kim, T. K., Lee, P., and Colman, R. F. (2003) Critical role of Lys212 and Tyr140 in porcine NADP-dependent isocitrate dehydrogenase. *J. Biol. Chem. 278*, 49323−49331.
(30) Cook, P. F., and Cleland, W. W. (1981) pH variation of isotope effects in enzyme-catalyzed reactions. 1. Isotope- and pH-dependent steps the same. *Biochemistry 20*, 1797−1805.
(31) Colman, R. F., and Chu, R. (1969) Deuterium solvent isotope effects in reactions catalyzed by isocitrate dehydrogenase. *Biochem. Biophys. Res. Commun. 34*, 528−535.
(32) Hermes, J. D., Roeske, C. A., O'Leary, M. H., and Cleland, W. W. (1982) Use of multiple isotope effects to determine enzyme mechanisms and intrinsic isotope effects. Malic enzyme and glucose-6-phosphate dehydrogenase. *Biochemistry 21*, 5106−5114.
(33) Nelson, D. L., and Cox, M. M. (2005) *Lehninger Principles of Biochemistry*, 4th ed., W. H. Freeman and Co., New York.
(34) Ottolina, G., Riva, S., Carrea, G., Danieli, B., and Buckmann, A. F. (1989) Enzymatic synthesis of [4R-2H]NAD(P)H and [4S-2H]NAD(P)H and determination of the stereospecificity of 7α- and 12α-hydroxysteroid dehydrogenase. *Biochim. Biophys. Acta 998*, 173−178.
(35) Thorsness, P. E., and Koshland, D. E., Jr. (1987) Inactivation of isocitrate dehydrogenase by phosphorylation is mediated by the negative charge of the phosphate. *J. Biol. Chem. 262*, 10422−10425.
(36) Hurley, J. H., Dean, A. M., Sohl, J. L., Koshland, D. E., Jr., and Stroud, R. M. (1990) Regulation of an enzyme by phosphorylation at the active site. *Science 249*, 1012−1016.
(37) Goncalves, S., Miller, S. P., Carrondo, M. A., Dean, A. M., and Matias, P. M. (2012) Induced Fit and the Catalytic Mechanism of Isocitrate Dehydrogenase. *Biochemistry 51*, 7098−7115.
(38) Xu, X., Zhao, J., Xu, Z., Peng, B., Huang, Q., Arnold, E., and Ding, J. (2004) Structures of human cytosolic NADP-dependent isocitrate dehydrogenase reveal a novel self-regulatory mechanism of activity. *J. Biol. Chem. 279*, 33946−33957.
(39) Vinekar, R., and Ghosh, I. (2009) Determination of phosphorylation sites for NADP-specific isocitrate dehydrogenase from *Mycobacterium tuberculosis*. *J. Biomol. Struct. Dyn. 26*, 741−754.
(40) Dang, L., White, D. W., Gross, S., Bennett, B. D., Bittinger, M. A., Driggers, E. M., Fantin, V. R., Jang, H. G., Jin, S., Keenan, M. C., Marks, K. M., Prins, R. M., Ward, P. S., Yen, K. E., Liau, L. M., Rabinowitz, J. D., Cantley, L. C., Thompson, C. B., Vander Heiden, M.

G., and Su, S. M. (2009) Cancer-associated IDH1 mutations produce 2-hydroxyglutarate. *Nature 462*, 739−744.
(41) Yang, B., Zhong, C., Peng, Y., Lai, Z., and Ding, J. (2010) Molecular mechanisms of "off-on switch" of activities of human IDH1 by tumor-associated mutation R132H. *Cell Res. 20*, 1188−1200.
(42) Pietrak, B., Zhao, H., Qi, H., Quinn, C., Gao, E., Boyer, J. G., Concha, N., Brown, K., Duraiswami, C., Wooster, R., Sweitzer, S., and Schwartz, B. (2011) A tale of two subunits: How the neomorphic R132H IDH1 mutation enhances production of αHG. *Biochemistry 50*, 4804−4812.